

Title:

Ischemia in tumors induces early and sustained phosphorylation changes in stress kinase pathways but does not affect global protein levels

Philipp Mertins^{a,1,2}, Feng Yang^{b,1}, Tao Liu^{b,1}, DR Mani^{a,1}, Vladislav A. Petyuk^{b,1}, Michael A. Gillette^{a,1}, Karl R. Clouser^a, Jana W. Qiao^a, Marina A. Gritsenko^b, Ronald J. Moore^b, Douglas A. Levine^c, Reid Townsend^d, Petra Erdmann-Gilmore^d, Jacqueline E. Snider^d, Sherri R. Davies^d, Kelly V. Ruggles^e, David Fenyo^e, R. Thomas Kitchens^d, Shunqiang Li^d, Narciso Olvera^c, Fanny Dao^c, Henry Rodriguez^f, Daniel W. Chan^g, Daniel Liebler^h, Forest Whiteⁱ, Karin D. Rodland^b, Gordon B. Mills^j, Richard D. Smith^b, Amanda G. Paulovich^k, Matthew Ellis^d and Steven A. Carr^{a,2}

On behalf of the Clinical Proteomic Tumor Analysis Consortium (CPTAC)

^aThe Broad Institute of MIT and Harvard, Cambridge, MA 02142

^bBiological Sciences Division, Pacific Northwest National Laboratory, Richland, WA 99352

^cGynecology Service/Department of Surgery, Memorial Sloan-Kettering Cancer Center, New York, NY 10065

^dDepartment of Medicine, Washington University, St. Louis, MO 63110

^eDepartment of Biochemistry, New York University Langone Medical Center, New York, NY 10016

^fNational Cancer Institute, National Institutes of Health, Bethesda, MD 20892

^gDepartment of Pathology, The Johns Hopkins Medical Institutions, Baltimore, MD 21287

^hDepartment of Biochemistry, Vanderbilt University School of Medicine, Nashville, TN 37232

ⁱDepartment of Biological Engineering, Massachusetts Institute of Technology, Cambridge, MA 02139

^jDepartment of Systems Biology, The University of Texas MD Anderson Cancer Center, Houston, TX 77030

^kFred Hutchinson Cancer Research Center, Seattle, WA 98109

¹These authors contributed equally to this work.

²To whom correspondence may be addressed: scarr@broad.mit.edu and pmertins@broadinstitute.org

Running title: Cold ischemia induces phosphoproteome alterations in tumors

The abbreviations used are: iTRAQ, isobaric tags for relative and absolute quantification; HCD, higher-energy collisional dissociation; TCGA, The Cancer Genome Atlas; NCI-CPTAC, National Cancer Institute's Clinical Proteomic Tumor Analysis Consortium; PTM, post-translational modification; PDX, patient-derived xenograft; IMAC, immobilized metal affinity chromatography; RPPA, reverse-phase protein array;

Abstract:

Protein abundance and phosphorylation convey important information about pathway activity and molecular pathophysiology in diseases including cancer, providing biological insight, informing drug and diagnostic development, and guiding therapeutic intervention. Analyzed tissues are usually collected without tight regulation or documentation of ischemic time. To evaluate the impact of ischemia, we collected human ovarian tumor and breast cancer xenograft tissue without vascular interruption and performed quantitative proteomics and phosphoproteomics after defined ischemic intervals. While the global expressed proteome and most of the >25,000 quantified phosphosites were unchanged after 60 minutes, rapid phosphorylation changes were observed in up to 24% of the phosphoproteome, representing activation of critical cancer pathways related to stress response, transcriptional regulation and cell death. Both pan-tumor and tissue-specific changes were observed. The demonstrated impact of pre-analytical tissue ischemia on tumor biology mandates caution in interpreting stress-pathway activation in such samples, and motivates reexamination of collection protocols for phosphoprotein analysis.

Keywords: Cold ischemia; proteome; phosphoproteome; phosphorylation; tumor tissue; delayed freezing; ovarian cancer; breast cancer; iTRAQ quantification; stress response pathway; p38 kinase

Introduction:

Genomic analysis of thousands of tumor samples from multiple cancer types is currently being carried out by consortia such as the Cancer Genome Atlas (TCGA) and the International Cancer Genome Consortium. These studies are yielding new insights into the biology of breast (1), brain (2), colon (3), lung (4), ovarian (5) and endometrial cancers (6, 7). In clinical trial settings, tumor biopsies are also being characterized to identify the molecular basis for drug response and to identify therapeutic targets (8). There is growing recognition that proteomic characterization of genetically annotated samples could provide complementary as well as unique information on cancer biology and signaling that is inaccessible by DNA and RNA analysis alone. In response to this perspective, reverse-phase protein array (RPPA) technology (9) has been incorporated into the analysis pipeline for TCGA samples. RPPA is a highly parallelized, chip-based dot-blot approach employing very well characterized anti-protein and anti-phosphopeptide antibodies. The power of proteomics in the context of TCGA has recently been highlighted by the ability of RPPA to identify new molecular taxonomies in breast cancer subtypes not discernible by genomics (1). A limitation of RPPA is that only around 200 antibodies are currently demonstrated to work well by this methodology.

We hypothesized that concurrent and complementary evaluation of the functional proteomes (including posttranslational modifications, PTMs) of tumors will improve our ability to diagnose, treat and prevent cancers through a better understanding of the molecular basis of these diseases, especially when integrated and analyzed together with the comprehensive genomic characterization information. Recent advances in the preparation of samples and their quantitative analysis by mass spectrometry-based proteomics and phosphoproteomics now yield data sets covering nearly half of the predicted proteome and identifying many thousands of phosphopeptides (10-14). These advances have sparked efforts utilizing state-of-the-art proteomics to characterize the proteomes and define changes in the posttranslational modification landscape of tumor samples. The National Cancer Institute's Clinical Proteomic Tumor Analysis Consortium (NCI-CPTAC) is therefore characterizing the proteomes of large numbers of breast, colon and ovarian tumor samples that have been genetically characterized by the TCGA program.

A concern faced by the CPTAC program is that the samples provided by TCGA for proteomic analysis were not obtained with proteomic studies in mind. Importantly, the

total duration of ischemia prior to sample freezing is generally unknown in TCGA samples but frequently spans tens of minutes to over an hour. The total ischemia duration comprises a period of warm ischemia corresponding to the time from blood vessel ligation to surgical excision, and cold ischemia corresponding to the delay-time to freezing post excision (usually a mix of transportation time to pathology and pathological analyses). Until now, the effect of cold ischemia on the stability of proteins and phosphosites has primarily been studied only for selected candidate proteins and phosphosites for which high quality antibodies were available. A study employing AQUA, a quantitative immunofluorescence technique, found slightly increased expression of hypoxia inducible factor but no changes in protein abundance of the four breast cancer biomarker proteins ER, PR, HER2 and Ki67 over a time-span of up to 7 hours, though signal reduction occurred in a subset of samples at longer intervals up to 48 hours of cold ischemia (15). In another study employing immunohistochemistry, the breast cancer biomarker proteins ER, PR and Her2 were found to be stable for up to 2 hours at room temperature (16). Evidence from RPPA studies evaluating the time course of changes induced by cold ischemia have shown that, while total protein levels and levels of many phosphoproteins are constant, phosphorylation stoichiometry of specific proteins can change, in some cases significantly (9, 17). For example, Espina et al. used 55 phosphosite-specific antibodies in RPPA format to show that in various tissues, including breast, ovary, colon and endometrium, cold ischemia can cause up to a two-fold variation in phosphorylation abundance and that these processes can be augmented by phosphatase inhibitors and reduced by kinase inhibitors (17) or heat stabilization (18). However, due to clinical sample handling limitations, the earliest time points evaluated in this study occurred between 4 and 40 minutes after tissue resection with an average time to cryopreservation of 19.3 minutes (17). The duration of blood vessel ligation, a common procedure in nearly all surgeries, was not noted and so the actual total ischemia times (warm ischemia plus cold ischemia) may have been longer. Hennessy et al. analyzed the effects of cold ischemia in breast cancer tumor samples using RPPA and found 21 of 82 proteins and phosphoproteins demonstrated a time-dependent instability at room temperature between 6 and 24 h of cold ischemia, but exhibited few effects at earlier time-points (9). Gundish et al. used both RPPA and LC-MS/MS to analyze a time course of cold ischemia in normal liver tissue from mouse and rat (34). No significant changes were observed in the phosphoproteome after up to 60 minutes of cold ischemia, in agreement with Hennessy et al. In the LC-MS/MS study by Gundisch et

al. ca. 1,700 phosphosites were quantified, but no statistically significant alterations of individual phosphosites over 60 minutes of cold ischemia were found. A few other unbiased mass spectrometry-based proteomic studies of cold ischemia have been reported. These studies identified a small number of proteins that changed in abundance (primarily degradation presumably via proteolysis) after long (> 3 h) periods of cold ischemia (19, 20). For example, Li et al. using two-dimensional fluorescence difference gel electrophoresis in conjunction with mass spectrometry identified 26 proteins that changed over 48 hours of cold ischemia time, chiefly by degradation (20). The sample collection and analysis approaches used in most of these studies did not permit assessment of changes within the one-hour interval investigated in our study.

Before embarking on analyses of PTM's in TCGA-profiled tumor samples, we wanted to better understand the potential effects of ischemia on the proteome and phosphoproteome of tumor tissue. Here we describe our time course studies of patient-derived xenografts of human breast cancer tumors and patient-derived ovarian cancer tumors. Tumor tissues were excised prior to vascular ligation to accurately define the ischemia time, and were prepared centrally using a cryopulverization method that maintained the tissue in a frozen state. Samples were analyzed using a common sample processing workflow for global, quantitative proteome and phosphoproteome analysis using iTRAQ chemical mass tag labeling for quantification (11, 21) and state-of-the art high performance, multidimensional LC-MS/MS on high performance mass spectrometers for data collection.

Experimental Procedures:

Preparation of ovarian tumor samples for proteomic analysis:

After obtaining consent to IRB-approved protocols, tissue was collected from four patients' high-grade serous ovarian carcinoma. Immediately after resection the tumors were dissected into four contiguous and adjacent strips each no larger than 10 x 3 x 3 mm. Tumor strips were placed into cryovials and frozen in liquid nitrogen at specified time points.

Generation and preparation of xenograft tumor samples for proteomic analysis:

All human tissues for these experiments were processed in compliance with NIH regulations and institutional guidelines, approved by the Institutional Review Board at

Washington University. All animal procedures were reviewed and approved by the Institutional Animal Care and Use Committee at Washington University in St. Louis. Patient-derived xenograft tumors (PDX tumors) from established basal (WHIM6) and luminal (WHIM20) breast cancer subtypes were raised subcutaneously in 8 week old NOD.Cg-*Prkdc*^{scid} *Il2rg*^{tm1Wjl}/SzJ mice (Jackson Labs, Bar Harbor, Maine) as previously described (22, 23). Tumors from each animal were harvested by surgical excision at approximately 1.5 cm³, rapidly divided into 4 pieces, and snap-frozen by immersion in a liquid nitrogen bath at times 0 (~ 30s), 5, 30 and 60 minutes post-excision.

Protein extraction, digestion, labeling and mass spectrometry analysis of peptides from patient-derived ovarian tumors and breast cancer PDX models

Proteins extracted from tumor tissues (~50 mg tissue weight for ovarian, ~100 mg tissue weight for breast cancer xenograft) were reduced, alkylated and subjected to enzyme digestion. Peptides were labeled with 4-plex iTRAQ reagents and separated using an off-line high pH (7.5 or 10) reversed-phase column. Fractions were collected and concatenated (14, 24) into 24 fractions, 5% of which was analyzed by LC-MS/MS for quantitative global proteomics measurement. The remaining (95%) of each of the 24 fractions was further concatenated into 12 fractions and phosphopeptides enriched using immobilized metal (Fe^{3+}) affinity chromatography (IMAC) prior to LC-MS/MS analysis. Peptides from ovarian cancer samples were analyzed using a nanoLC system coupled to an LTQ-Orbitrap-Velos MS (Thermo Scientific) at Pacific Northwest National Laboratories. Peptides from breast cancer PDX samples were analyzed using a nanoLC system coupled to a Q Exactive MS (Thermo Scientific) at the Broad Institute. All mass spectrometry data were analyzed using the Spectrum Mill software package v4.1 beta (Agilent Technologies, Santa Clara, CA). Peptide identifications and quantification information were further combined into protein and phosphosite tables. Statistical analysis of cold-ischemia regulated proteins and phosphosites by kinetic modeling and moderated F-test was performed using the R software environment (version 2.15.2).

RPPA Analysis:

Protein expression or phosphorylation was measured by reverse phase protein arrays (RPPAs) as previously described (9).

More detailed experimental Methods are presented in the Supporting Information Materials and Methods.

Results:

Experimental design to study effects of cold ischemia on the proteome and phosphoproteome of ovarian and breast cancer samples using a quantitative LC-MS/MS

In this study we analyzed the effect of delayed freezing on protein and phosphoprotein stability in tumor samples derived from four ovarian cancer patients and two breast cancer patient-derived xenografts (PDX; one basal and one luminal) (22). Blood vessels were not ligated prior to tumor excision, thereby eliminating effects of warm ischemia. Individual tumor samples were cut into four sections, which were subsequently stored at room temperature for predefined time intervals (Fig. 1A). Upon partitioning, the first section was frozen immediately with a time span of less than one minute from excision to freezing in liquid nitrogen. Later time point sections were left at room temperature and frozen after 5, 30 or 60 minutes, to investigate the kinetics of changes in the proteome and phosphoproteome caused by delayed freezing.

The ovarian tumors were obtained from four individual cancer patients with high-grade serous ovarian carcinoma and the four time point samples per patient were derived from four contiguous, adjacent portions of the same tumor. While the use of surgically excised tumors was desirable because it recapitulated a typical biospecimen collection scenario, it was recognized that intra-tumor heterogeneity (e.g. genetic differences or differences in non-tumor elements) could result in proteomic variations not related to ischemic time. To mitigate this concern, as well as to extend our analysis to another tumor type, we carried out the same ischemia time course study in xenografts from two distinct molecular phenotypes of breast cancer, ER+ (luminal) and ER- (basal-like). Tumor xenografts have less cellular infiltration and therefore are less heterogeneous than tumors excised from patients. Additionally, since total tumor material was not limiting for the breast cancer xenograft samples, we pooled 5 to 10 xenografts (derived from the same luminal and basal-like tumors) at each time point to dampen effects of biological variability. We generated three individual pools for the basal as well as the luminal

breast cancer xenograft samples which can be considered as biological replicates since each individually grown xenograft tumor was present only in one pooled sample.

To analyze the proteome and phosphoproteome, frozen tumor samples were cryofractured, and proteins were extracted with an 8 M urea buffer and digested into peptides using trypsin (Fig. 1B). For relative quantification across the four ischemia time points of each tumor, peptide samples were chemically labeled with iTRAQ reagents and subsequently combined into a single sample. iTRAQ-labeling covalently attaches isotope-coded isobaric mass tags to primary amine groups at the N-termini of peptides and Lysine-side chains. Upon fragmentation in the mass spectrometer, reporter ions at defined masses are released and the ratio of these reporter ions to one another enables relative quantification (21). After iTRAQ-labeling, peptide samples were fractionated using basic reversed-phase liquid chromatography (RPLC) to reduce overall sample complexity per fraction and thus increase depth of coverage (24). Basic RPLC fractions were combined in a non-contiguous manner into 24 proteome and 12 phosphoproteome fractions with 5% of the total material contributing to the proteome analysis and 95% to the phosphoproteome analysis. Phosphopeptides were further enriched using immobilized metal affinity chromatography (IMAC).

Cold ischemia induces significant changes in protein phosphorylation, but no changes in overall protein abundance

Our quantitative LC-MS/MS platform was extensively tested within the CPTAC program to assure reproducibility of peptide identification and quantification for proteome and phosphoproteome analysis. Average Pearson correlations for process replicate analysis of breast cancer xenograft tumors were $r = 0.808$ on the proteome and $r = 0.812$ on the phosphoproteome level. Using our platform, nearly 15,000 different proteins and up to 26,000 distinct phosphosites were reproducibly quantified in at least two tumor samples (Table 1, Supporting Information (SI) Tables S1 and S2). Among these were 86 phospho-tyrosine (pTyr)-sites and 202 pTyr-sites that were reproducibly measured in the ovarian and breast cancer tumor samples, respectively. The total protein and phosphosite counts are in general higher for xenograft compared to the human ovarian tumor samples in part because the xenograft samples contain additional proteins from mouse stroma (no more than 20 % based on genomic analysis), but also because the breast tumor samples were analyzed using a more sensitive mass spectrometer (see SI

Materials and Methods). To identify consistent ischemia-induced alterations we employed two complementary statistical tests. The first approach assumes that most of the changes are unidirectional and governed by the first order chemical kinetics rule. In this method we used a non-linear regression with three degrees of freedom that fit initial abundance, final abundance and a kinetic constant. The second approach did not rely on an explicit assumption that the changes follow a particular pattern. Instead, each time point was treated as an independent group in an ANOVA analysis, with statistical significance being assessed using a moderated F-test. This allowed capturing additional trends that are not unidirectional. Proteins and phosphosites with a Benjamini-Hochberg corrected p-value <0.01 in either test (i.e., the union of significant proteins/phosphosites) are considered to be regulated by ischemia. In this analysis, we have used a relatively stringent p-value of 0.01 (compared to the usual p-value of 0.05) for statistical significance in order to minimize false positive results. As the number of samples studied here is relatively small, borderline p-values could change in significance as more samples are analyzed. As with any statistical analysis, we expect that the list of phosphosites ranked as significant includes some false positives and false negatives. We provide tables of p-values for all proteins and phosphosites (Tables S1 and S2) to facilitate assessment of significance not based on a specific p-value threshold.

We did not detect a single significantly regulated protein with altered abundance levels at up to 60 minutes of ischemia time for any of the ovarian tumor samples or for the luminal and basal-like PDX samples. In contrast, significant ischemia-induced changes in the phosphoproteome were observed for all analyzed tumor types (Table 1). The kinetics-based regression and the moderated F-test (ANOVA) analysis identified a largely overlapping set of regulated phosphorylation-sites for a given tumor; only a small number of changes were identified uniquely by only one of the statistical tests (Fig. S1). Response to cold ischemia was asymmetrically distributed, with more phosphorylation sites being up-regulated than down-regulated for all of the tumors (Fig. 2). The largest changes in ischemia-induced phosphorylation were observed for the luminal breast cancer PDX which exhibited 19.8 % up-regulated and 4.5% down-regulated phosphorylation-sites at 1 % FDR (Table 1). The ischemic behavior of the ovarian and basal-like breast cancer samples, which have been proposed to be molecularly similar (1), was less dramatic, with 4.6 % and 5.7 % up-regulated and 1.2 % and 3.9 % down-regulated phosphorylation-sites, respectively. For these three tumor types, only the tails of the density distribution of Log2 ratios increased with ischemic time. In contrast, the

global median of the luminal breast cancer phosphoproteome was shifted to increased abundance levels (Fig. 2). The effects of cold ischemia on pTyr-sites were comparable to those observed on pSer/pThr-sites in the whole phosphoproteome analysis. In the ovarian cancer and basal-like breast cancer samples 8 % of all pTyr-sites were up-regulated and 2-4 % down-regulated. Ischemia-regulated pTyr-sites were more frequent in the luminal tumors with 13.6 % up- and 5.4 % down-regulated sites.

Kinetic analysis of phosphoproteome dynamics reveals phosphosites that change as early as 5 minutes after sample excision

To identify temporal trends we used fuzzy c-means clustering (25) to assign membership of all regulated phosphorylation sites from all three tumor types in 9 different clusters with different temporal profiles. These clusters were further combined into 3 up- (U) and 3 down- (D) regulated groups (Fig. 3A). In addition, we have calculated the median half-activation times for all sites that belong to one of these groups to determine at what time these sites had reached 50% of their maximum alteration (saturation). The early groups U1 and D1 showed a T_{1/2} of 3 and 2 minutes, and the late groups U3 and D3 of 46 and 34.4 minutes, respectively. The number of phosphorylation sites grouped into the different temporal clusters varied across all three tumor types (Fig. 3B). Enrichment analysis of Gene Ontology Biological Process (GO BP) terms for the up-regulated clusters revealed activation of MAPK cascade and Ras signaling pathways for the early group U1 (Fig. 3C). Specific activation of transcriptional regulators was observed for the medium group U2, and regulation of chromatin modification and assembly (among other biological processes) for the late group U3. In the down-regulated clusters D1-D3, regulation of Rho, Ras and GTPase signal transduction and regulation of cytoskeleton organization were among the more highly enriched GO BP terms. Fewer GO BP terms were enriched for groups D1-D3 due to the smaller number of down-regulated phosphorylation sites. The response kinetics in the different tumor types were slightly offset, with some kinases appearing in different temporal clusters for the different tumor types (Fig. S2).

Common phosphoproteome changes induced by cold ischemia are observed independent of tumor type

To define the set of ischemia-regulated phosphorylation sites that are observed in common across the ovarian and the two breast cancer samples, we plotted all time point ratios measured in at least two different tumor types and calculated inter-tumor Pearson

correlation coefficients (Fig. 4A). The inter-tumor type correlation increased with longer ischemia time and reached r values of 0.6 at 30 and 60 minutes. The intra-tumor type correlation (which for breast constituted replicate analyses of differing pools) for the 60 minute time point ratios was $r = 0.66$ for the basal-like breast tumors, $r = 0.80$ for the luminal breast tumors and $r = 0.39$ for the ovarian tumor samples. As expected, we observed a higher degree of biological variability for the individual ovarian tumor samples compared to the pooled replicate samples for the basal-like and luminal breast xenograft samples (Fig. S3). Averaging values across samples conserved commonly regulated effects and improved the inter-tumor compared to the intra-tumor correlation for ovarian cancer. Across all three tumor types we found 137 phosphorylation-sites to be commonly up-regulated and 21 to be down-regulated (Fig. 4B,C; Table 2). These 158 commonly regulated phosphorylation-sites were identified as being regulated with a FDR <0.01 in each individual tumor type. Therefore it is very unlikely that any of the sites observed to be regulated in common across the three different tumor types are false positives.

We also analyzed enrichment of KEGG pathways among all cold ischemia-regulated phosphoproteins for each tumor type and found that most enriched pathways were detected in at least two of the tumor types (Fig. S4). Activation patterns of MAPK and the ErbB signaling pathway were common to all three tumor types. Among the most enriched tumor-specific biological processes were the activation of RIG-1-like receptor signaling pathway in basal breast cancer, up-regulation of mTOR signaling, WNT signaling and adherens junctions in luminal breast cancer, and up-regulation of vascular smooth muscle contraction in ovarian cancer. Among the three tumor types evaluated, the luminal breast cancer samples exhibited the largest number and highest percentage of uniquely regulated phosphosites. This indicates that there may be tissue-specific changes across lineages that should ideally be assessed prior to analysis of patient samples in each tumor lineage.

Cold ischemia induces changes in kinase phosphorylation status across all major kinase subfamilies

Next, we investigated how different protein kinase subfamilies were affected by cold ischemia induced by delayed freezing of tumor tissue. We quantified phosphorylation sites on more than 360 human protein kinase isoforms in this study. In total, 14 protein kinases with regulated phosphorylation sites were detected in all three tumor types (Fig.

5A): EGFR (pT693), ARAF (T181, S186), Erk1/MAPK3 (Y204), Erk2/MAPK1 (T185, Y187), p38a/MAPK14 (Y182), PKCD (S304), PRKD2 (S214), PRKD3 (S731), NEK7 (S187), NEK9 (S332), RSK2 (T577), RSKL1 (S583), mTOR (S1261) and Sgk269/PEAK1 (S1217). These commonly regulated kinases, as well as tumor-specifically regulated kinases, were evenly distributed among all major kinase subfamilies (Fig. 5A). We found that 48 % of all kinases contained a regulated site for the luminal breast tumors in contrast to the ovarian and basal breast tumors with 17 % and 29 %, respectively. This is consistent with the overall higher level of ischemia-induced changes observed in the luminal subtype.

Common ischemia-regulated phosphoproteins belong to an EGFR/MAPK signaling module

We further analyzed the set of 139 commonly regulated phosphoproteins for modules of proteins that physically interact with each other or have been described as kinase-substrate pairs. Using curated protein-protein interaction information from the STRING database (26) and site-specific kinase-substrate relationship information from the PhosphoSitePlus database (www.phosphosite.org) (27), we were able to group 30 of these ischemia-regulated phosphoproteins into a functional protein network (Fig. 5B). This network was dominated by proteins involved in EGFR and MAPK signaling. The EGFR was up-regulated at T693, a site involved in receptor internalization (28) and suppression of EGF-induced JNK activation (29). Distal to EGFR, the adaptor protein SHC1 and the phosphatase PTPN12 were detected, which bind to EGFR and are involved in MAPK activation. P38/MAPK14, Erk1/MAPK3 and Erk2/MAPK1 were up-regulated on phosphosites in their activation loops and sites on proteins downstream of Erk1/MAPK3 such as stathmin 1 (STMN1) and capicua (CIC) were also up-regulated. As EGFR T693 phosphorylation has a negative effect on its downstream signaling, and p38/MAPK14, Erk1/MAPK3 and Erk2/MAPK1 can directly phosphorylate the EGFR at this site (28), we suggest that phosphorylation of the T693 site in EGFR could be involved in negative feedback regulation of the EGFR due to cold ischemia.

We also mapped regulated phosphosites to the KEGG database JNK & p38 MAP kinase pathways (Fig. S5). The p38/MAPK14 pathway was up-regulated in all tumor

types, whereas the JNK pathway was observed to be up-regulated only in the luminal breast cancer tumors. Of note, JNK is also known as stress activated kinase or SAPK and p38 has also been characterized as a stress response kinase. Interestingly, DNA and RNA sequencing analysis of the luminal breast tumor revealed a splice site mutation in the stress-pathway kinase MAP3K1 that generates an out of frame transcript (22). MAP3K1 phosphorylation was not observed to be upregulated in the luminal PDX, in contrast to the basal line. However, contrary to expectations for loss of MAP3K1 function, the JNK pathway was strongly activated by ischemia (Fig. S5). This suggests a MAP3K1-independent activation mechanism for the JNK pathway that could increase cell survival when ischemia-like conditions occur in an evolving, growing tumor, similar to events proposed in cardiac myocytes (30). Specific phosphorylation of apoptosis-inducing caspases (CASP2/3/9) was also only observed in the luminal breast cancer tumors.

Among the other commonly regulated phosphoproteins (Fig. 5B) a group of proteins was found that function in mRNA export (NUP214), translation (EIF4G1) and polyA-tail shortening (PARN, TNKS1BP1). Pleiotropic regulators of mitotic progression such as Nek7 and Nek9 were also regulated on phosphosites by ischemia, as were transcriptional regulators (TRIM28) and pro-apoptotic regulators (BAD).

Comparison of results obtained by quantitative mass spectrometry-based proteomics and reversed-phase protein arrays (RPPA)

Since RPPA measurements are widely used to investigate cancer-relevant signaling pathways, we compared the results obtained by quantitative LC-MS/MS with results obtained by RPPA on the same samples of all tumors in the current study. The RPPA studies used 40 phosphosite-specific antibodies, 10 of which are to pTyr-sites. We successfully identified 25 and quantified 23 of the 40 phosphosites measured by these antibodies in our phosphoproteome analysis using LC-MS/MS, including 7 of 10 pTyr-sites. We observed a good correlation of results for the ovarian, basal-like breast and luminal breast cancers with Pearson correlation values of $r = 0.79$, 0.83 and 0.75 , respectively (Fig. S6; Table S3). Of the 15 phosphosites detected by RPPA but not by LC-MS/MS, 10 are located in surrounding sequences that upon tryptic digestion would yield peptides that are ill-suited to mass spectrometric identification; i.e. peptides shorter than 5 amino acids or longer than 30 amino acids with only a single basic residue. Lack of detection of the remaining five (of 40) phosphosites by LC-MS/MS may be due to

higher sensitivity of the phosphoantibodies for these sites or unexpected cross reactivity of the antibodies leading to false positive identification by RPPA. Protein level quantification by RPPA for 87 proteins across all tumor types revealed in agreement with our MS data no changes on protein level due to cold ischemia (Table S3). Across all tumor types 85 of these proteins were identified with 2 or more peptides and 80 proteins were quantified in at least two tumors by mass spectrometry.

Discussion:

In this study, we systematically analyzed the effect of up to one hour of cold ischemia time on the stability of the proteome and phosphoproteome of ovarian and breast cancer tumor samples. Cold ischemia is a complex physiological perturbation that integrates the effects of tissue stress, hypoxia, hypoglycemia, acidosis, hypothermia, and electrolyte disturbance. It is of special relevance in tissue profiling as both a pervasive and a comparatively modifiable pre-analytical variable. The one hour endpoint we chose to study is particularly pertinent because it represents a convergence of three important parameters: the cold ischemic time allowed in TCGA tumor tissue acquisition protocols; the upper limit of cold ischemic time recommended by the American Society of Clinical Oncology guidelines for breast cancer tumor marker assessment (31); and the upper bound on intervals typically reported for those aspects of sample processing that contribute to routine cold ischemia, including specimen transport to pathology and macroscopic evaluation by a pathologist (19).

The extent of the proteome and phosphoproteome detected and quantified in our study is the largest in any ischemia study and among the largest in any proteomics experiment to date, owing to advances in sample preparation, use of latest generation LC-MS instrumentation and statistically rigorous data analysis methods. Our comprehensive proteome analysis, which greatly expands on prior studies of the consequences of cold ischemia on protein expression (15, 16), revealed that none of the >10,000 proteins detected and quantified changed in abundance due to cold ischemia in a time span of up to one hour post excision. However, due to the inability of conventional “bottom-up” MS-based proteomics technology to analyze the integrity of intact proteins (as samples are digested to peptides prior to analysis), we cannot exclude the possibility that limited proteolysis such as apoptotic regulation by caspases occurs at early time points of cold ischemia. Protein stability across this level of coverage, which approaches the

anticipated scale of the expressed proteome, provides compelling evidence that the results of quantitative global proteomics are robust to the common vagaries of post-excision tissue handling in the surgical and pathology suites. These findings are similar to those obtained in a study on mRNA integrity in breast cancer tissue where no substantial effects on mRNA yield/integrity or transcript expression were detected after either 40 minutes or three hours of cold ischemia (32).

While the global proteome is remarkably stable, the impact of cold ischemia on the phosphoproteome is more pronounced, with some alterations occurring within five minutes of removal of the tissue from its blood supply, the earliest post-baseline time point investigated in this study. Between 6 % and 24 % of the more than 25,000 distinct, chiefly pSer or pThr phosphosites we identified were observed to be regulated by cold ischemia in one or more of the three tumor types we analyzed. Importantly, our study therefore identifies a large subset of the phosphoproteome that remains relatively stable and can be accurately measured, even in samples subjected to a full hour of cold ischemia. These results suggest that phosphoproteome analysis of the TCGA tumor samples can proceed with an acceptable expected yield of biologically relevant phosphoprotein data.

We observed a common phosphosite signature of cold ischemia response in the ovarian and breast cancer tumors consisting of 137 up- and 21 down-regulated sites that underwent up to 6-fold alterations in abundance (Table 2, Fig. S7). The strong increase in phosphorylation across tumor types induced by cold ischemia mainly involved activation of MAPK stress response pathways, apoptosis and transcriptional regulation. Among the ischemia-regulated proteins were proteins such as p38/MAPK14 (Y182) and Erk1/MAPK3 (Y204) that have previously been shown by RPPA to change due to ischemia (17). Although some phosphosites were observed to decrease in common across all three tumor types examined, the signature of increased phosphorylation was far stronger, suggesting that kinase activation is a more pervasive response than loss of phosphorylation due to increased phosphatase activity. Minor differences in the kinetics of protein phosphorylation were observed between the different tumor types, which may be due to different baseline tissue oxygenation or vascularization. The common phosphosite signature of cold ischemia response we observed, or one derived from it, could, in principle, be used to identify tumor samples that underwent strong cold ischemic stress conditions, and potentially to estimate the duration of the shock period.

Such information could then inform interpretation of experimental results. The generalizability of the signature to other tumors and tissues has not yet been demonstrated, but is readily testable. We are developing targeted MS-based assays (MRM-MS or similar) employing stable isotope labeled internal standard peptides for a number of the ischemia-marker candidates to facilitate such analyses (33). Furthermore, while warm ischemia is not explicitly addressed in this study, the nature of the tissue insult is in many respects comparable to that of cold ischemia, and it is plausible that our data could provide the foundation of a global ischemia signature. The importance of establishing such quality standards for samples used for proteomic and phosphoproteomic analysis is clear.

Our results are in partial agreement with a previous report by Espina and colleagues who found by RPPA analysis that apoptosis, hypoxia, and proliferation-related proteins increase transiently within the initial 30 min post excision (17). The effects observed in our study were larger in amplitude and did not return to baseline, possibly because of tissue-specific differences or the longer total ischemia time in the RPPA study. In a recent LC MS/MS-based analysis of delayed freezing of mouse and rat livers, Gundisch et al. found that most phosphoproteome changes are diffuse and unpredictable and can be minimized when samples are kept on ice prior to fixation (34). The lack of a common cold ischemia response in this study may be explained by different stress response mechanisms in healthy and diseased tissues. Our results also contrast with those of Pinhel and coworkers (35), who reported that delaying time to fixation post-resection significantly decreased the immunoreactivity of p-Akt and p-ERK1/2, two potentially useful diagnostic markers of receptor tyrosine kinase pathway activation. This discrepancy is likely due to the very long latency to effective formalin fixation of the resection samples analyzed in that study. The increased phosphorylation of Erk1 we observed was supported by both LC-MS/MS and RPPA analyses, adding confidence in the activation of MAPK pathways by cold ischemia.

An important potential caveat to our study is that significant regional heterogeneity in particular signaling molecules across the tumor could, if present, contribute to apparent differences in the effects of ischemia on phosphosite stability. Of necessity, different portions of tumor material were analyzed at each of the time points. Furthermore, heterogeneity in protein expression across tumors has long been observed by IHC and more recently by other approaches including exome sequencing (36). Although regional

heterogeneity is a legitimate concern, it is unlikely a critical determinant in our study. We do not observe substantial regional variability in the total number of proteins and phosphosites identified across time points in our study. This may be due to the fact that the volume of the samples analyzed at each time point was relatively large, and for the breast cancer samples included regions pooled across multiple tumors, reducing concerns with micro-heterogeneity. Alternatively, under-sampling by the LC-MS/MS system due to the complexity of the tumor samples may reduce our ability to detect such differences. However, the kinetics of change observed in different phosphosites are more consistent with the monotonic perturbation of increased ischemia time than with the random effects expected of heterogeneity. Notably, a prior direct analysis of intra-tumoral heterogeneity by RPPA failed to detect major changes across different parts of the tumor (9).

In addition to common stress responses we also observed tumor-specific responses to cold ischemia. The variability between stability of phosphosites in luminal breast, basal breast and serous ovarian cancers, together with coordinate regulation of many phosphosites, suggest that phosphosite stability will be pathway-, context- and lineage-dependent. For example, we observed very strong induction of protein phosphorylation in a luminal breast tumor that contains a splice site mutation in the gene for the stress kinase MAP3K1. This correlation of a mutated gene to a strong phosphoproteome phenotype may indicate that the full extent of ischemic response is dependent on the genetic repertoire of each tumor, a suggestion further supported by the greater biological variability observed in the responses of individual ovarian tumors. The effects of specific genetic events can be more clearly studied with a larger number of genetically annotated PDX models, which would also permit additional perturbations to be studied including those induced by therapeutic approaches. Together, these observations argue for caution and circumspection in the interpretation of phosphoproteomic data from TCGA samples, as well as from samples populating the vast majority of valuable “collaborative” repositories collected with conventional constraints on cold ischemia time.

Because tissues undergoing excision are alive and able to mount coordinated responses to insults, variation in ischemia time can either mask or artifactually amplify underlying pathways of importance. For example, proteins in stress response pathways, including those we have shown to be regulated by cold ischemia, have been implicated in cancer progression and drug resistance (37, 38). Certainly, phosphoprotein

measurements used to guide clinical decision-making should be specifically studied for stability within the parameters of their particular sample acquisition protocol. While somewhat greater latitude may be allowed research specimens, at a minimum our results suggest that the total duration of cold ischemia (and by extension warm ischemia) should be carefully noted for samples to be analyzed by any proteomic methods. Whenever possible, cancer and other tissue specimens should be frozen as soon after resection as possible since cold ischemia-induced changes in the phosphoproteome become evident after just a few minutes. If warm ischemic effects are at all comparable to the cold ischemic effects described here, biopsies taken pre-operatively or intra-operatively before the interruption of vascular supply may be needed for accurate characterization of the tumor phosphoproteome. If minimally ischemic acquisition and immediate freezing are beyond institutional capacity or fall outside clinical sample handling protocols, the commonly regulated ischemia phosphorylation sites identified in this study may be monitored, potentially through use of targeted MS-based assays (33), to identify samples that may have been subjected to increased ischemic stress. A metric based on targeted measurement of this set would allow suspect samples to be flagged, though it would not necessarily provide guidance as to which specific phosphosites remained interpretable. The utility of the set of phosphosite markers that we have identified as commonly perturbed in ischemic breast and ovarian cancer will require additional studies of other tumor types to establish whether such a tool would be of general use.

Acknowledgments:

This work was supported in whole or in part, by National Institutes of Health grants from the National Cancer Institute grant numbers U24CA160034 (to S. A. C. and A.G.P.); U24CA160019 (to R. D. S. and K. D. R.), U24CA160035 (to M.J.E. and R.R.T.); U24CA159988 (to D.L.); and U24CA160036 (to D.C.) as part of the NCI Clinical Proteomics Tumor Analysis Consortium. The PDX models were developed through grants to Matthew J Ellis by Susan G. Komen for the Cure (BCTR0707808 and

KG090422). The Siteman Cancer Center Tissue Procurement Core is supported by NCI P30CA091842. Tissue procurement core was supported NCI 3P50 CA68438. The HAMLET Core was supported by CTSA grant UL1 RR024992. The ovarian cancer sample collection was supported by the Chia Family Foundation. The RPPA analysis was supported by MD Anderson Cancer Center Support Grant (CCSG) CA016672 from National Institutes of Health and PO1CA099031, U54CA112970, KG081694 and P30 CA16672 to Gordon Mills.

Author contributions:

P.M., F.Y., T.L., M.A.G., D.A.L., R.T., S.R.D., P.G., H.R., D.C., D.L., K.D.R., G.B.M., R.D.S., A.G.P., M.E., F.W. and S.A.C. Study design and development; P.M., F.Y., T.L., J.W.Q., M.A.G., R.J.M., S.R.D., P.G., J.E.S., R.T.K., S.L., N.O. and F.D. performed research; D.R.M., V.A.P., K.R.C., K.V.R. and D.F. contributed new analytic tools; P.M., F.Y., T.L., D.R.M., V.A.P., M.A.G., K.R.C., K.V.R., D.F., G.B.M., M.A. and S.A.C. analyzed data; P.M., F.Y., T.L., D.R.M., V.A.P., M.A.G., D.A.L., G.B.M., K.D.R., A.G.P., M.E. and S.A.C. wrote the paper.

References:

1. Cancer Genome Atlas N (2012) Comprehensive molecular portraits of human breast tumours. *Nature* 490(7418):61-70.
2. Cancer Genome Atlas Research N (2008) Comprehensive genomic characterization defines human glioblastoma genes and core pathways. *Nature* 455(7216):1061-1068.
3. Cancer Genome Atlas N (2012) Comprehensive molecular characterization of human colon and rectal cancer. *Nature* 487(7407):330-337.
4. Cancer Genome Atlas Research N (2012) Comprehensive genomic characterization of squamous cell lung cancers. *Nature* 489(7417):519-525.
5. Cancer Genome Atlas Research N (2011) Integrated genomic analyses of ovarian carcinoma. *Nature* 474(7353):609-615.
6. Cancer Genome Atlas Research N, et al. (2013) Integrated genomic characterization of endometrial carcinoma. *Nature* 497(7447):67-73.
7. Salvesen HB, et al. (2009) Integrated genomic profiling of endometrial carcinoma associates aggressive tumors with indicators of PI3 kinase activation. *Proc Natl Acad Sci U S A* 106(12):4834-4839.
8. Ellis MJ, et al. (2012) Whole-genome analysis informs breast cancer response to aromatase inhibition. *Nature* 486(7403):353-360.
9. Hennessy BT, et al. (2010) A Technical Assessment of the Utility of Reverse Phase Protein Arrays for the Study of the Functional Proteome in Non-microdissected Human Breast Cancers. *Clin Proteomics* 6(4):129-151.
10. Wisniewski JR, Dus K, & Mann M (2013) Proteomic workflow for analysis of archival formalin-fixed and paraffin-embedded clinical samples to a depth of 10 000 proteins. *Proteomics Clin Appl* 7(3-4):225-233.
11. Mertins P, et al. (2012) iTRAQ labeling is superior to mTRAQ for quantitative global proteomics and phosphoproteomics. *Mol Cell Proteomics* 11(6):M111 014423.
12. Huttlin EL, et al. (2010) A tissue-specific atlas of mouse protein phosphorylation and expression. *Cell* 143(7):1174-1189.
13. Lundby A, et al. (2012) Quantitative maps of protein phosphorylation sites across 14 different rat organs and tissues. *Nat Commun* 3:876.
14. Mertins P, et al. (2013) Integrated proteomic analysis of post-translational modifications by serial enrichment. *Nat Methods* 10(7):634-637.
15. Neumeister VM, et al. (2012) Quantitative assessment of effect of preanalytic cold ischemic time on protein expression in breast cancer tissues. *J Natl Cancer Inst* 104(23):1815-1824.
16. Yildiz-Aktas IZ, Dabbs DJ, & Bhargava R (2012) The effect of cold ischemic time on the immunohistochemical evaluation of estrogen receptor, progesterone receptor, and HER2 expression in invasive breast carcinoma. *Mod Pathol* 25(8):1098-1105.
17. Espina V, et al. (2008) A portrait of tissue phosphoprotein stability in the clinical tissue procurement process. *Mol Cell Proteomics* 7(10):1998-2018.
18. Ahmed MM & Gardiner KJ (2011) Preserving protein profiles in tissue samples: differing outcomes with and without heat stabilization. *J Neurosci Methods* 196(1):99-106.
19. Gundisch S, et al. (2012) Variability of protein and phosphoprotein levels in clinical tissue specimens during the preanalytical phase. *Journal of proteome research* 11(12):5748-5762.

20. Li J, et al. (2013) Intrinsic indicators for specimen degradation. *Lab Invest* 93(2):242-253.
21. Ross PL, et al. (2004) Multiplexed protein quantitation in *Saccharomyces cerevisiae* using amine-reactive isobaric tagging reagents. *Mol Cell Proteomics* 3(12):1154-1169.
22. Li S, et al. (2013) Endocrine Therapy Resistant ESR1 Variants revealed by Genomic Characterization of Breast Cancer Derived Xenografts. *Cell Reports* in press.
23. Ding L, et al. (2010) Genome remodelling in a basal-like breast cancer metastasis and xenograft. *Nature* 464(7291):999-1005.
24. Wang Y, et al. (2011) Reversed-phase chromatography with multiple fraction concatenation strategy for proteome profiling of human MCF10A cells. *Proteomics* 11(10):2019-2026.
25. Kumar L & M EF (2007) Mfuzz: a software package for soft clustering of microarray data. *Bioinformation* 2(1):5-7.
26. Franceschini A, et al. (2013) STRING v9.1: protein-protein interaction networks, with increased coverage and integration. *Nucleic Acids Res* 41(Database issue):D808-815.
27. Hornbeck PV, et al. (2012) PhosphoSitePlus: a comprehensive resource for investigating the structure and function of experimentally determined post-translational modifications in man and mouse. *Nucleic Acids Res* 40(Database issue):D261-270.
28. Winograd-Katz SE & Levitzki A (2006) Cisplatin induces PKB/Akt activation and p38(MAPK) phosphorylation of the EGF receptor. *Oncogene* 25(56):7381-7390.
29. Bagowski CP, Stein-Gerlach M, Choidas A, & Ullrich A (1999) Cell-type specific phosphorylation of threonines T654 and T669 by PKD defines the signal capacity of the EGF receptor. *EMBO J* 18(20):5567-5576.
30. Dougherty CJ, et al. (2002) Activation of c-Jun N-terminal kinase promotes survival of cardiac myocytes after oxidative stress. *Biochem J* 362(Pt 3):561-571.
31. Harris L, et al. (2007) American Society of Clinical Oncology 2007 update of recommendations for the use of tumor markers in breast cancer. *J Clin Oncol* 25(33):5287-5312.
32. Hatzis C, et al. (2011) Effects of tissue handling on RNA integrity and microarray measurements from resected breast cancers. *J Natl Cancer Inst* 103(24):1871-1883.
33. Gillette MA & Carr SA (2013) Quantitative analysis of peptides and proteins in biomedicine by targeted mass spectrometry. *Nat Methods* 10(1):28-34.
34. Gundisch S, et al. (2013) Delayed times to tissue fixation result in unpredictable global phosphoproteome changes. *Journal of proteome research* 12(10):4424-4434.
35. Pinhel IF, et al. (2010) Extreme loss of immunoreactive p-Akt and p-Erk1/2 during routine fixation of primary breast cancer. *Breast Cancer Res* 12(5):R76.
36. Gerlinger M, et al. (2012) Intratumor heterogeneity and branched evolution revealed by multiregion sequencing. *N Engl J Med* 366(10):883-892.
37. Gauthier ML, et al. (2007) Abrogated response to cellular stress identifies DCIS associated with subsequent tumor events and defines basal-like breast tumors. *Cancer Cell* 12(5):479-491.
38. Schiff R, et al. (2000) Oxidative stress and AP-1 activity in tamoxifen-resistant breast tumors *in vivo*. *J Natl Cancer Inst* 92(23):1926-1934.

39. Huang da W, Sherman BT, & Lempicki RA (2009) Systematic and integrative analysis of large gene lists using DAVID bioinformatics resources. *Nat Protoc* 4(1):44-57.
40. Manning G, Whyte DB, Martinez R, Hunter T, & Sudarsanam S (2002) The protein kinase complement of the human genome. *Science* 298(5600):1912-1934.
41. Shannon P, et al. (2003) Cytoscape: a software environment for integrated models of biomolecular interaction networks. *Genome Res* 13(11):2498-2504.

Figure legends:

Figure 1: Quantitative proteome and phosphoproteome analysis of human ovarian tumors and xenograft breast tumors subjected to controlled ischemia.

(A) Experimental design to study effects of post-excision delay time before freezing across 4 time points. After excision tumor samples were cut into 4 equal pieces and incubated for the indicated times at room temperature before freezing. A total of 4 different ovarian tumors and 3 pooled breast cancer xenograft samples for the basal as well as the luminal subtype were analyzed. All of these samples are biologically distinct and can be considered as biological replicates. **(B) Quantitative proteomics and phosphoproteomics workflow using 4-plex iTRAQ labeling.** Tumor samples were cryofractured and proteins extracted with urea lysis buffer prior to digestion into peptides using trypsin. Peptide samples derived of 4 different ischemic time points were labeled using iTRAQ reagents, mixed equably and separated using high pH reversed-phase chromatography. Fractions were combined in a non-contiguous way into 24 fractions for proteome analysis (5% of total material) and 12 fractions for phosphoproteome analysis (95% of total material). Ovarian cancer samples were analyzed on an LTQ-Orbitrap Velos and xenograft breast cancer samples on a Q Exactive mass spectrometer. Phosphosite and protein identification and quantification were achieved using Spectrum Mill.

Figure 2: Global proteome analysis reveals no changes in protein abundance level, but specific alterations in the phosphoproteome induced by ischemia. Density plots are shown for averaged phosphosite iTRAQ ratios (labeled with “pSTY”) and protein iTRAQ ratios (small inserts) for the ovarian cancer (OC) samples, as well as the basal-like and luminal breast cancer (BC) samples. Only phosphosites/proteins were plotted that were quantified in ≥ 3 ovarian tumors and ≥ 2 basal-like or luminal tumor samples.

Figure 3: Temporal dynamics of phosphorylation changes resulting from cold ischemia. (A) Fuzzy c-means clustering of temporal profiles for all regulated phosphosites observed in the ovarian and breast cancer samples. We detected 6 up-regulated (U) clusters, which were further grouped pairwise into early (U1), middle (U2) and late clusters (U3), and 3 down-regulated (D1, D2, D3) clusters using a fuzzyfication parameter $m = 1.6$. Phosphosites were assigned to each cluster with a membership value $\alpha > 0.7$. $T_{1/2}$ indicates the median over all half-maximum time points for all phosphosites within a cluster. Half-maximum time points were determined by first-order kinetic modeling analysis. **(B) Number of regulated phosphosites assigned to each cluster for the ovarian and breast cancer tumors.** **(C) Gene enrichment analysis of regulated human phosphoproteins across early, middle and late clusters.** We used DAVID Bioinformatics Resources 6.7 (<http://david.abcc.ncifcrf.gov/>) (39) to test for enrichment of Gene Ontology biological processes (GO BP) in each cluster compared to a list of all proteins containing non-regulated sites using a modified Fisher's exact test (EASE score). GO BP categories with $p < 0.01$ and a minimum occurrence of ≥ 10 genes/proteins were called significant. P-values were $-\log_{10}$ transformed and the transformed values for each annotation were plotted as a heat map in Gene-E (<http://www.broadinstitute.org/cancer/software/GENE-E>).

Figure 4: Ischemia induces common phosphorylation events in ovarian and basal-like/luminal breast cancer tumor samples. (A) Scatter plots of averaged phosphosite ratios (5:0, 30:0 and 60:0) over ≥ 3 ovarian tumors (OC), and ≥ 2 basal-

like (BA) or ≥2 luminal (LU) breast cancer samples. X and Y indicate which tumor type is plotted on the respective axis. Inter-tumor Pearson correlation coefficients are indicated for each tumor type comparison. **(B, C) Venn diagrams of the overlap of up-regulated (B) and down-regulated (C) phosphosites between ovarian and basal-like/luminal breast cancer samples.**

Figure 5: Stress response kinases are affected by cold ischemia. (A) Kinases detected with and without regulated phosphosites were mapped in a dendrogram of the human kinome (40) using KinomeCluster (<http://depts.washington.edu/iscrmwik/kinome-cluster/>). Ischemia regulated kinases were observed across all major kinase subfamilies. (B) Protein-protein interaction and kinase-substrate network of phosphoproteins commonly regulated in all analyzed ovarian and breast cancer samples. High confidence, experimentally validated protein-protein interaction information was obtained from the STRING protein interaction database (<http://string-db.org/>) (26). Kinase-substrate relationships were derived from the Phosphosite.org database (<http://www.phosphosite.org>) (27). Protein-protein interaction and site-specific kinase-phosphosite relationships were illustrated using Cytoscape (www.cytoscape.org) (41) with blue edges indicating protein-protein interactions and red dashed arrows indicating kinase-substrate relationships. Up-regulated phosphosites are shown in green and down-regulated sites in red. Kinases are depicted as squares, whereas all other proteins appear as circles.

Table 1: Number of quantified and ischemia regulated phosphosites and proteins in ovarian and breast cancer tumors.

| | n tumor samples | Total | average per tumor sample | overlap in at least (n-1) samples | kinetics-based regression test* | moderated F-test* | union of both tests* | % regulated ** |
|---|-----------------|-------|--------------------------|-----------------------------------|---------------------------------|-------------------|----------------------|----------------|
| Quantified phosphorylation sites | | | | | | | | |
| Ovarian Cancer | 4 | 23607 | 13156 | 9443 | 307/97 | 386/63 | 432/111 | 4.6/1.2 |
| Basal Breast Cancer | 3 | 38366 | 27668 | 26211 | 1252/948 | 1156/633 | 1493/1027 | 5.7/3.9 |
| Luminal Breast Cancer | 3 | 34327 | 25814 | 25102 | 4154/820 | 4220/962 | 4977/1139 | 19.8/4.5 |
| Quantified proteins | | | | | | | | |
| Ovarian Cancer | 4 | 9498 | 7550 | 6985 | 0/0 | 0/0 | 0/0 | 0/0 |
| Basal Breast Cancer | 3 | 17158 | 14989 | 14970 | 0/0 | 0/0 | 0/0 | 0/0 |
| Luminal Breast Cancer | 3 | 14224 | 12641 | 12679 | 0/0 | 0/0 | 0/0 | 0/0 |

* significant regulation at a kinetics-based regression test or moderated F-test FDR p<0.01

** percent regulated phosphosites and proteins within overlap dataset

Table2: Commonly regulated phosphorylation-sites that were significantly altered due to cold ischemia in ovarian cancer as well as basal and luminal breast cancer

| GI-number | Protein name | Gene name | Phosphosite | Sequence ¹ | Average iTRAQ ratio 60/0 min (Log2 scale) | | |
|-----------|---|-----------|-------------|---------------------------|---|--------------|----------------|
| | | | | | Ovarian | Basal Breast | Luminal Breast |
| 87299628 | Biorientation of chromosomes in cell division protein 1-like | BOD1L | S800 | KLsVLGK | 1.47 | 2.65 | 4.59 |
| 4504517 | Heat shock protein beta-1 | HSPBL2 | S15 | GPswDPFR | 3.72 | 2.01 | 2.39 |
| 61743954 | Neuroblast differentiation-associated protein AHNK | AHNK | S3426 | VSMPDVNLNsPK | 2.66 | 2.48 | 2.87 |
| 48255933 | Non-histone chromosomal protein HMG-14 | HMGN1 | S7 | RKVsSAEGAAKEEPK | 1.93 | 2.43 | 2.97 |
| 192807323 | Transcription activator BRG1 isoform A | SMARCA4 | S1382 | EVYSDsLTEKQWLK | 2.10 | 2.05 | 2.95 |
| 22355917 | Protein LYRIC | MTDH | S298 | LSSQIqASGEK | 2.56 | 2.37 | 2.10 |
| 5032179 | Transcription intermediary factor 1-beta | TRIM28 | S489 | KPVRVsLER | 1.89 | 1.76 | 3.19 |
| 14670350 | General transcription factor II-I isoform 1 | GTF2I | S722 | GREFsFEAWNAK | 1.63 | 2.50 | 2.55 |
| 259906018 | Apoptotic chromatin condensation inducer in the nucleus isoform 2 | ACIN1 | S864 | KPSlslTTESLK | 1.89 | 2.38 | 2.32 |
| 37577122 | Ubiquitin-conjugating enzyme E2 J1 | UBE2J1 | S184 | QlsFK | 2.35 | 1.54 | 2.63 |
| 20357552 | Src substrate cortactin isoform a | CTTN | S432 | AELsYRGPVSGTEPEPVYSMEA | 2.40 | 1.82 | 1.86 |
| 38372909 | Lysine-specific demethylase 3B | KDM3B | S798 | APFEAVKRFsLDER | 1.71 | 1.58 | 2.65 |
| 14670350 | General transcription factor II-I isoform 1 | GTF2I | S103 | MsVDAVEIETLRK | 1.59 | 1.64 | 2.66 |
| 82659109 | E3 ubiquitin-protein ligase UBR4 | UBR4 | S1760 | HaStSSPADAK | 2.56 | 1.09 | 2.20 |
| 193083183 | Synaptopodin-2 isoform a | SYNPO2 | S1091 | SlsLPGR | 2.86 | 1.29 | 1.69 |
| 114842410 | Zinc finger CCCH domain-containing protein 11A | ZC3H11A | S290 | RKFsAGGDSDPPLKR | 0.99 | 2.14 | 2.66 |
| 9994185 | RNA-binding protein 7 | RBM7 | S204 | MNsYPYLADR | 1.62 | 1.73 | 2.41 |
| 40556376 | Putative oxidoreductase GLYR1 | GLYR1 | S130 | RKlsLSEGK | 1.81 | 2.37 | 1.51 |
| 281182404 | Gamma-taxilin isoform 1 | CXorf15 | S105 | NLVSPAYCT*QE*sREEIPGGEAR | 2.10 | 1.76 | 1.71 |
| 4507691 | Transformation/transcription domain-associated protein | TRRAP | S2033 | RGLsVDSAQEVKR | 1.93 | 1.93 | 1.61 |
| 41281917 | Protein polybromo-1 isoform 4 | PBRM1 | S948 | TySQCDSFK | 1.42 | 1.87 | 2.08 |
| 33356174 | Pinin | PNN | S66 | RGFsDGGGGPPAK | 1.62 | 1.57 | 2.16 |
| 4502193 | Serine/threonine-protein kinase A-Raf | ARAF | T181 S186 | QHEAPSNRPLNELLIPQGPSPR | 2.06 | 1.04 | 2.16 |
| 112421108 | Protein capicua homolog | CIC | S1389 | AiLGsYR | 2.15 | 1.25 | 1.83 |
| 21626468 | Zinc finger protein 638 | ZNF638 | S383 | NYGSQADIPRsPFGIVK | 2.14 | 1.09 | 1.97 |
| 61743954 | Neuroblast differentiation-associated protein AHNK | AHNK | S3411 | FKMPFLsSPK | 1.45 | 1.43 | 2.30 |
| 9994185 | RNA-binding protein 7 | RBM7 | S136 | SFsSPENFQR | 2.20 | 1.01 | 1.89 |
| 34996489 | PH-interacting protein | PHIP | S1315 | AQsYDIQAWKK | 1.66 | 1.41 | 1.95 |
| 5174545 | Myocyte-specific enhancer factor 2D | MEF2D | S121 | RAsEELDGLFR | 2.22 | 0.80 | 2.00 |
| 28872725 | 26S proteasome non-ATPase regulatory subunit 11 | PSMD11 | S14 | AQsLLSTDREASIDILHSIVKR | 1.63 | 1.48 | 1.86 |
| 20986514 | Mitogen-activated protein kinase 14 isoform 3 | MAPK14 | Y182 | HTDDEmTgYVATR | 1.38 | 1.77 | 1.74 |
| 7662238 | Apoptotic chromatin condensation inducer in the nucleus isoform 1 | ACIN1 | S825 | RKlsVSVATK | 1.00 | 1.78 | 2.08 |
| 65288071 | Tensin-3 | TNS3 | S1154 | ASEAASPLPDsPGDKLIVIK | 1.66 | 1.59 | 1.61 |
| 14670268 | Negative elongation factor E | RDBP | S51 | SLsEQPVMDTATAEQAK | 1.14 | 1.81 | 1.85 |
| 61676188 | E3 ubiquitin-protein ligase HUWE1 | HUWE1 | S2593 | LLGPsAAADILQLsSSLPLQSR | 1.73 | 1.30 | 1.76 |
| 190886437 | RaiBP1-associated Eps domain-containing protein 1 isoform b | REPS1 | S272 S273 | RQs*s*S*DDPWKTDEQRQYY | 2.07 | 1.21 | 1.48 |
| 82659109 | E3 ubiquitin-protein ligase UBR4 | UBR4 | S362 | T*G*TSSKEDDYESDAATIVQK | 1.92 | 1.05 | 1.70 |
| 4504517 | Heat shock protein beta-1 | HSPBL2 | S82 | QLsSGVSEIR | 1.60 | 1.08 | 1.98 |
| 42716280 | Vigilin | HDLBP | S645 | IlslQK | 2.01 | 1.26 | 1.31 |
| 14043072 | Heterogeneous nuclear ribonucleoproteins A2/B1 isoform B1 | HNRNPA2B1 | S212 | GGNFGFGDsR | 2.17 | 1.22 | 1.15 |
| 148596984 | Golgin subfamily B member 1 | GOLGB1 | S3010 | QAsPETsASPQDGSQLNVYETLLR | 1.70 | 1.31 | 1.50 |
| 51173720 | Peregrin isoform 1 | BRPF1 | T896 | Rt*s*VLFsk | 1.22 | 1.29 | 1.91 |
| 223890147 | Kinetochore-associated protein DSN1 homolog isoform 1 | DSN1 | S109 | RKsLHPiHQGITLSR | 2.05 | 1.06 | 1.30 |
| 116256352 | Tuberin isoform 1 | TSC2 | S1364 | VVsSEGGRPSVDSLFSQPSQLSK | 1.90 | 0.77 | 1.68 |
| 61743954 | Neuroblast differentiation-associated protein AHNK | AHNK | S5186 | VKTPs*FGIS*APQVSPDGVNVNLK | 1.58 | 1.22 | 1.55 |
| 4505611 | Poly(A)-specific ribonuclease PARN isoform 1 | PARN | S557 | NNsFTAPSTVGK | 1.72 | 1.13 | 1.49 |
| 24371248 | FUN14 domain-containing protein 2 | FUNDc2 | S151 | IRKsNQIPTEV | 2.21 | 1.22 | 0.90 |
| 116256352 | Tuberin isoform 1 | TSC2 | S1254 | SlsVPAASTAKPPPLPR | 1.39 | 1.03 | 1.90 |
| 20986531 | Mitogen-activated protein kinase 1 | MAPK1 | T185 Y187 | VADPDHDHTGFLtEyVATR | 1.54 | 1.44 | 1.33 |
| 262359929 | Protein ELYS | AHCTF1 | S1241 | IsFVEEDVHPK | 1.52 | 1.15 | 1.62 |
| 27597090 | Transcription elongation factor SPT6 | SUPT6H | S91 | KRTs*FDRLLEDDDFDIEENLGV | 1.72 | 1.11 | 1.45 |
| 13786127 | Cdc42 effector protein 4 | CDC42EP4 | S174 | RNGAAGPHsPDPLLDEQAFGDLT | 1.53 | 1.23 | 1.47 |
| 21361891 | SH2 domain-containing protein 4A isoform a | SH2D4A | S315 | TLsSSAQEDIIIRWFKEEQLPLR | 1.26 | 1.36 | 1.60 |
| 117553584 | AP-3 complex subunit delta-1 isoform 1 | AP3D1 | S567 | HRPsEADEEELAR | 1.56 | 1.50 | 1.14 |
| 208022661 | Nck-associated protein 5-like | NCKAP5L | S767 | VDLEPVsPR | 1.72 | 0.81 | 1.67 |
| 31377562 | HAUS augmin-like complex subunit 6 | HAUS6 | T584 | NQIPRIPENLITEIR | 1.97 | 0.78 | 1.43 |
| 61676188 | E3 ubiquitin-protein ligase HUWE1 | HUWE1 | S3116 | LFGHsSTSALSAILR | 2.15 | 0.65 | 1.25 |
| 4557896 | Myotubularin | MTM1 | S588 S590 | LSDPPTs*Ps*s*PSQmMPHVQTH | 1.73 | 0.94 | 1.34 |
| 14670268 | Negative elongation factor E | RDBP | S131 | sLYESFVSSSDRLR | 1.58 | 0.90 | 1.52 |
| 140161500 | Ankyrin repeat and SAM domain-containing protein 1A | ANKS1A | S620 | AELKLsR | 1.35 | 0.72 | 1.87 |
| 224451142 | Stathmin isoform b | STMN1 | S25 | ASQQAFELlsPR | 1.53 | 1.00 | 1.36 |
| 22027612 | TNF receptor-associated factor 2 | TRAF2 | S11 | AAASVTPPsLsLELLQPGFSK | 1.06 | 0.80 | 2.02 |
| 5032179 | Transcription intermediary factor 1-beta | TRIM28 | S473 | sGEGEVSLGLMR | 0.81 | 1.18 | 1.74 |
| 27597059 | DnaJ homolog subfamily C member 9 | DNAJC9 | S109 | KlsLEDIQAFEK | 1.09 | 0.89 | 1.70 |
| 4504919 | Keratin, type II cytoskeletal 8 | KRT8 | S475 | LvsESSDVLPLK | 1.10 | 1.31 | 1.24 |
| 21493029 | A-kinase anchor protein 13 isoform 2 | AKAP13 | S2561 | lSLRPSSLIEQEK | 0.79 | 1.13 | 1.73 |
| 110556636 | 182 kDa tankyrase-1-binding protein | TNKS1BP1 | S1029 | GSGGLFsPSTAHPVDPGALGQR | 1.94 | 0.87 | 0.79 |
| 51093863 | Niban-like protein 1 isoform 1 | FAM129B | S692 S696 | AAPEAs*s*PPAsPLQHLLPGK | 1.36 | 0.61 | 1.62 |
| 222136641 | Serine/threonine-protein kinase Nek9 | NEK9 | S332 | SsTVTEAPIAVTSR | 1.42 | 1.12 | 1.05 |
| 19424132 | Serine/threonine-protein kinase Nek7 | NEK7 | S187 | Ffssk | 1.19 | 1.07 | 1.28 |
| 7705373 | LIM domain and actin-binding protein 1 isoform b | LIMA1 | S604 | SRPFTVAASFQS*T*S*VKs*PK | 1.53 | 0.95 | 1.05 |
| 21070984 | Peptidyl-glycine alpha-amidating monooxygenase | PAM | S919 | GKGsGGNLNLGNFFASR | 1.61 | 0.93 | 0.98 |
| 5729858 | Nuclear receptor coactivator 2 | NCOA2 | S771 | LdsKTDPASTNK | 0.70 | 1.32 | 1.49 |
| 289577098 | Protein Shroom1 isoform 1 | SHROOM1 | S302 | LGDAFRPAsR | 1.37 | 1.21 | 0.92 |
| 14670268 | Negative elongation factor E | RDBP | S115 | SlsADDDLQESSRRPQRK | 0.94 | 1.28 | 1.28 |
| 87299628 | Biorientation of chromosomes in cell division protein 1-like | BOD1L | S635 | RLsESLHVVDENKNESKLER | 0.76 | 1.40 | 1.32 |
| 112421108 | Protein capicua homolog | CIC | S739 | SAAATsPAPHLVAGPLLGTVGK | 0.81 | 1.29 | 1.36 |
| 32261324 | SHC-transforming protein 1 isoform 2 | SHC1 | Y318 | ELFDDPSVNVQNLDK | 1.55 | 1.19 | 0.69 |
| 30023820 | Hypothetical protein LOC162427 | FAM134C | S26 | RDVsGSWER | 1.49 | 0.75 | 1.18 |
| 4759050 | Ribosomal protein S6 kinase alpha-3 | RPS6KA3 | T577 | AENGLLmtPCYTANFVAPEVLKR | 0.85 | 1.26 | 1.28 |

Table 2 (continued)

| GI-number | Protein name | Gene name | Phosphosite | Sequence ¹ | Average iTRAQ ratio 60/0 min (Log2 scale) | | |
|-----------|---|-------------|-------------|---------------------------|---|--------------|----------------|
| | | | | | Ovarian | Basal Breast | Luminal Breast |
| 301129165 | Death-inducer obliterator 1 isoform c | DIDO1 | S1456 | RNsVERPAEPVAGAATPSLVEQQ | 1.23 | 0.96 | 1.18 |
| 4826730 | Serine/threonine-protein kinase mTOR | MTOR | S1261 | LHVtTINLQK | 1.22 | 0.85 | 1.25 |
| 41281496 | Mediator of RNA polymerase II transcription subunit 24 isoform 1 | MED24 | S862 | LLsSNEDDANILSSPTDR | 1.16 | 1.24 | 0.92 |
| 120659782 | Serine/threonine-protein kinase D2 isoform A | PRKD2 | S214 | LGTSEELPCTAEELSR | 1.28 | 0.72 | 1.32 |
| 5031689 | Serine/threonine-protein kinase D3 | PRKD3 | S731 | IIGEKSFR | 0.76 | 0.94 | 1.60 |
| 262399371 | Transmembrane protein 201 isoform 1 | TMEM201 | S454 | ALsLGTIPSLTR | 1.22 | 0.92 | 1.13 |
| 48762920 | 6-phosphofructokinase, liver type | PFKL | S775 | TLsMDKGF | 1.02 | 1.13 | 1.09 |
| 6005884 | Translocon-associated protein subunit gamma | SSR3 | S105 | KLsEADNR | 1.42 | 1.18 | 0.63 |
| 54112429 | Dedicator of cytokinesis protein 7 | DOCK7 | S452 | T*T'sGDDACNLTSFR | 0.64 | 1.43 | 1.15 |
| 24430146 | Nuclear pore complex protein Nup153 | NUP153 | S516 | VQMTsPSSTGSPMFK | 0.85 | 1.16 | 1.19 |
| 10190682 | Chromobox protein homolog 8 | CBX8 | S256 | RQDsDLVQCGVTSPSSAEATGK | 0.96 | 1.22 | 1.01 |
| 61743954 | Neuroblast differentiation-associated protein AHNAK | AHNAK | S135 | LKsEDGVEGDLGETQSR | 1.18 | 1.07 | 0.90 |
| 166795297 | Cytoplasmic dynein 1 light intermediate chain 1 | DYNC1L1 | S516 | KPVTVSPPTT*s*PTEGEAS | 1.15 | 0.86 | 1.13 |
| 98986457 | Host cell factor 1 | HCF1 | S666 | TITLVksPISVPVGALSNLGK | 1.46 | 0.73 | 0.89 |
| 33946327 | Nuclear pore complex protein Nup214 | NUP214 | S1023 | TPsIQPSLLPHAAFPFAK | 0.89 | 0.91 | 1.29 |
| 38569480 | MKL/myocardin-like protein 2 | MKL2 | S882 | SGEISLPIKEEPsPISK | 1.38 | 0.24 | 1.46 |
| 7662647 | Phosphatidylserine synthase 1 | PTDSS1 | S11 | TLsKDDVNLY | 0.93 | 0.78 | 1.37 |
| 13899253 | Uridine-cytidine kinase 1 isoform a | UCK1 | S253 | TfsEPGDHPGmLTSGKR | 0.95 | 0.95 | 1.13 |
| 269847874 | Probable ATP-dependent RNA helicase YTHDC2 | YTHDC2 | S1201 | Ks*sADTEFSDECTTAER | 0.97 | 1.02 | 1.04 |
| 23346420 | Nuclear factor related to kappa-B-binding protein | NFKB | S323 | KGsLAALYDVLALK | 1.19 | 1.09 | 0.70 |
| 190341074 | Pyridoxal-dependent decarboxylase domain-containing protein 1 | PDXDC1 | S710 | LPQKQPKFRsLR | 1.01 | 1.03 | 0.94 |
| 71040094 | Arfaptin-1 isoform 1 | ARFIP1 | S132 | KWsLNTYK | 1.32 | 0.65 | 0.99 |
| 112382252 | Spectrin beta chain, brain 1 isoform 2 | SPTBN1 | S14 | TSSISGPLsPAYTQGVPYNYNQLE | 0.93 | 0.65 | 1.37 |
| 150418007 | E3 SUMO-protein ligase RanBP2 | RANBP2 | S1509 | KQsLPATSIPTPASFK | 1.59 | 0.67 | 0.67 |
| 4503579 | Band 4.1-like protein 2 isoform a | EPB41L2 | S598 | EVRsPTKAPHQLOLIEGKK | 1.12 | 0.59 | 1.19 |
| 151101292 | Thioredoxin-related transmembrane protein 1 precursor | TMX1 | S270 | QRsLGPSLATDKS | 1.39 | 0.82 | 0.67 |
| 109638745 | Transforming growth factor beta-1-induced transcript 1 protein | TGFB1II | S164 | LMAssLSDFR | 0.98 | 0.90 | 0.97 |
| 24308171 | Zinc finger protein 280C | ZNF280C | S80 | GIKSEPHsPGIPEIFR | 1.09 | 0.68 | 1.04 |
| 167234419 | Thyroid hormone receptor-associated protein 3 | THRAP3 | S248 S253 | ERsPALKsPLQSVVVR | 1.06 | 0.70 | 1.02 |
| 153252201 | Zinc transporter ZIP6 isoform 1 | SLC39A6 | S478 | YESQLsTNEEK | 0.83 | 0.95 | 1.00 |
| 29725609 | Epidermal growth factor receptor isoform a precursor | EGFR | T693 | ELVEPltPSGEAPQNALLR | 1.11 | 0.78 | 0.88 |
| 19745184 | Cyclic AMP-responsive element-binding protein 1 isoform B | CREB1 | S142 | ILNDLsSDAPGVPR | 1.08 | 0.67 | 1.02 |
| 19923723 | Ribosomal protein S6 kinase delta-1 isoform a | RPS6KC1 | S583 | AHELKFPPNNDPEAVS*s*PR | 0.84 | 0.85 | 1.07 |
| 91718899 | Mitogen-activated protein kinase 3 isoform 1 | MAPK3 | Y204 | IDAEHDHTGFLTeVATR | 0.88 | 0.86 | 1.00 |
| 52630440 | Peptidyl-prolyl cis-trans isomerase KFBP8 | KFBP8 | S297 | SCsLVLEHQPDNIK | 0.94 | 0.86 | 0.91 |
| 117189975 | Heterogeneous nuclear ribonucleoproteins C1/C2 isoform a | HNRNPC | S115 | SAAEmYGSVTEHPSpSPLLSSFD | 0.90 | 0.89 | 0.91 |
| 38788260 | Nucleosome-remodeling factor subunit BPTF isoform 2 | BPTF | S1310 | CPKQNsIENDIEEK | 0.93 | 1.00 | 0.75 |
| 197304775 | TBC1 domain family member 5 isoform b | TBC1D5 | S522 | SEsmPVQLNK | 0.91 | 0.57 | 1.18 |
| 14141152 | Heterogeneous nuclear ribonucleoprotein M isoform a | HNRNPM | S637 | GNFGGSFAGsFGGGAGGHAPGVA | 1.12 | 0.69 | 0.78 |
| 183396804 | Regulation of nuclear pre-mRNA domain-containing protein 2 | RPRD2 | S1099 | RmsGEPIQTVESIRVPGK | 0.56 | 0.94 | 1.09 |
| 20070205 | Ladinin-1 | LAD1 | S356 | LPPVTLQVKIPSKEEADMsPTQ | 0.93 | 0.85 | 0.80 |
| 13559514 | Phosphatidylinositol 4-kinase type 2-alpha | PI4K2A | S462 | SSsESYTQSFSQR | 1.23 | 0.72 | 0.63 |
| 21626466 | Matrin-3 isoform a | MATR3 | S188 | RDsFDRR | 0.80 | 0.76 | 1.00 |
| 71274144 | AT-hook DNA-binding motif-containing protein 1 | AHDC1 | S1187 | ANsEASSSEQQSSLSSLEK | 1.18 | 0.71 | 0.65 |
| 10835069 | Bcl-2 antagonist of cell death | BAD | S75 | HSsYPAGTEDDEGMGEESPFR | 1.03 | 0.66 | 0.84 |
| 4505581 | Interferon-inducible double stranded RNA-dependent protein kinase activator A | PRKRA | S18 | EDsGTFSLGK | 0.89 | 0.55 | 1.06 |
| 57634536 | La-related protein 4B | LARP4B | S568 | TLsADASVNTLPVVVS | 0.90 | 1.02 | 0.54 |
| 209180457 | Target of Myb protein 1 isoform 2 | LOC10012852 | T164 | GLEFPMTDLMLSPHPR | 1.12 | 0.67 | 0.64 |
| 150417986 | Brefeldin A-inhibited guanine nucleotide-exchange protein 2 | ARFGEF2 | S1024 | EREGsLK | 1.23 | 0.48 | 0.72 |
| 52426745 | E3 ubiquitin-protein ligase CBL | CBL | S619 | ELTNRHsLPFSLPSQMEPR | 1.07 | 0.72 | 0.63 |
| 47519639 | Microtubule-associated protein 4 isoform 1 | MAP4 | S825 | sPSTLKP | 0.98 | 0.64 | 0.63 |
| 5453710 | LIM and SH3 domain protein 1 | LASP1 | S146 | mGPSGEGmEPERRDsQDGSSY | 0.87 | 0.97 | 0.36 |
| 20986531 | Mitogen-activated protein kinase 1 | MAPK1 | Y187 | VADPDHDTGFLTeVATR | 0.62 | 1.03 | 0.53 |
| 31377782 | Protein kinase C delta type | PRKCD | S304 | Sd*sAS*SEPVGIVYQGFKE | 0.71 | 0.63 | 0.76 |
| 48928019 | NEDD4-binding protein 1 | N4BP1 | S300 | KQFsLENVQEGLILDAK | 0.76 | 0.75 | 0.55 |
| 221219024 | Pleckstrin homology-like domain family B member 1 isoform a | PHLDB1 | S430 | TFsDGLATR | 1.04 | 0.74 | 0.25 |
| 114688046 | TBC1 domain family member 4 | TBC1D4 | S566 | AKRsLTSSLNENFSR | 1.18 | 0.40 | 0.05 |
| 157384982 | Transducin-like enhancer protein 3 isoform a | TLE3 | T328 | NDAPIPGTSTTPGLR | -0.67 | -0.67 | -0.48 |
| 333108224 | Afadin isoform 1 | MLLT4 | S215 | TlsNPENVVmK | -0.80 | -0.90 | -0.84 |
| 48928019 | NEDD4-binding protein 1 | N4BP1 | T242 | AGtPVSELTK | -1.08 | -0.76 | -0.79 |
| 194595509 | Spectrin alpha chain, brain isoform 1 | SPTAN1 | S1029 | KLDPAQs*AS*R | -1.12 | -0.63 | -0.97 |
| 4507641 | Tumor protein D53 isoform 1 | TPD52L1 | S149 | sFEER | -0.81 | -1.67 | -0.31 |
| 11321634 | CD2-associated protein | CD2AP | S458 | sVDFDSLTVR | -0.77 | -0.96 | -1.09 |
| 115430211 | Phosphatase and actin regulator 4 isoform 1 | PHACTR4 | S291 | NSNPVIAELSQAINSGTLLSKPsPP | -1.15 | -0.92 | -0.78 |
| 92087055 | PERQ amino acid-rich with GFY domain-containing protein 1 | GIGYF1 | S137 | sIEEGDGAFFGR | -1.22 | -0.98 | -0.82 |
| 148368962 | Pseudopodium-enriched atypical kinase 1 | SGK269 | S1217 | GLDIESYdsLERPLRK | -1.22 | -1.21 | -0.71 |
| 302699245 | Eukaryotic translation initiation factor 4 gamma 1 isoform 6 | EIF4G1 | S1084 | ITKPGsIDSNNQLFAPGGR | -1.29 | -1.24 | -0.64 |
| 196114951 | Tyrosine-protein phosphatase non-receptor type 12 isoform 1 | PTPN12 | S449 | KVPLQEGPKsFDGNTLLNR | -1.23 | -1.34 | -0.80 |
| 61743954 | Neuroblast differentiation-associated protein AHNAK | AHNAK | S379 | LKGPQITGPsLEGDLGLK | -1.59 | -0.94 | -0.85 |
| 115298682 | Protein PRRC2C | BAT2L2 | T2673 | AFGSGIDIKPGtPPIAGR | -1.23 | -1.18 | -1.02 |
| 21070997 | Stromal interaction molecule 1 precursor | STIM1 | S575 | LPDsPALAK | -1.77 | -0.76 | -1.22 |
| 115298682 | Protein PRRC2C | BAT2L2 | T2682 | ST*tPTSSPFR | -1.62 | -1.27 | -0.89 |
| 10863895 | Thymosin beta-10 | TMSB10 | T23 | TEtQEKNTLPTK | -1.43 | -1.36 | -1.19 |
| 47519639 | Microtubule-associated protein 4 isoform 1 | MAP4 | S941 | VGsTENIKHQPGGGR | -1.80 | -1.32 | -1.09 |
| 224994221 | SH3 domain-binding protein 2 isoform b | SH3BP2 | S484 | SfSFKEKPR | -1.57 | -0.84 | -1.90 |
| 30089916 | Phosphofuran acidic cluster sorting protein 1 | PACS1 | S519 | QLsKPLSER | -1.54 | -1.88 | -1.85 |
| 62198235 | Drebrin-like protein isoform b | DBNL | T291 | QLQPETHFGREPAAlSRRP | -1.26 | -2.45 | -1.70 |
| 156766050 | Protein AHNAK2 | AHNAK2 | S842 | FKMpsFGVSApGK | -1.94 | -2.41 | -2.14 |

1) Lower case s,t, and y indicate phosphorylated residues in peptide sequence; all phosphosites are fully localized except where indicated with an asterisk; m = oxidized methionine

Figure 1:

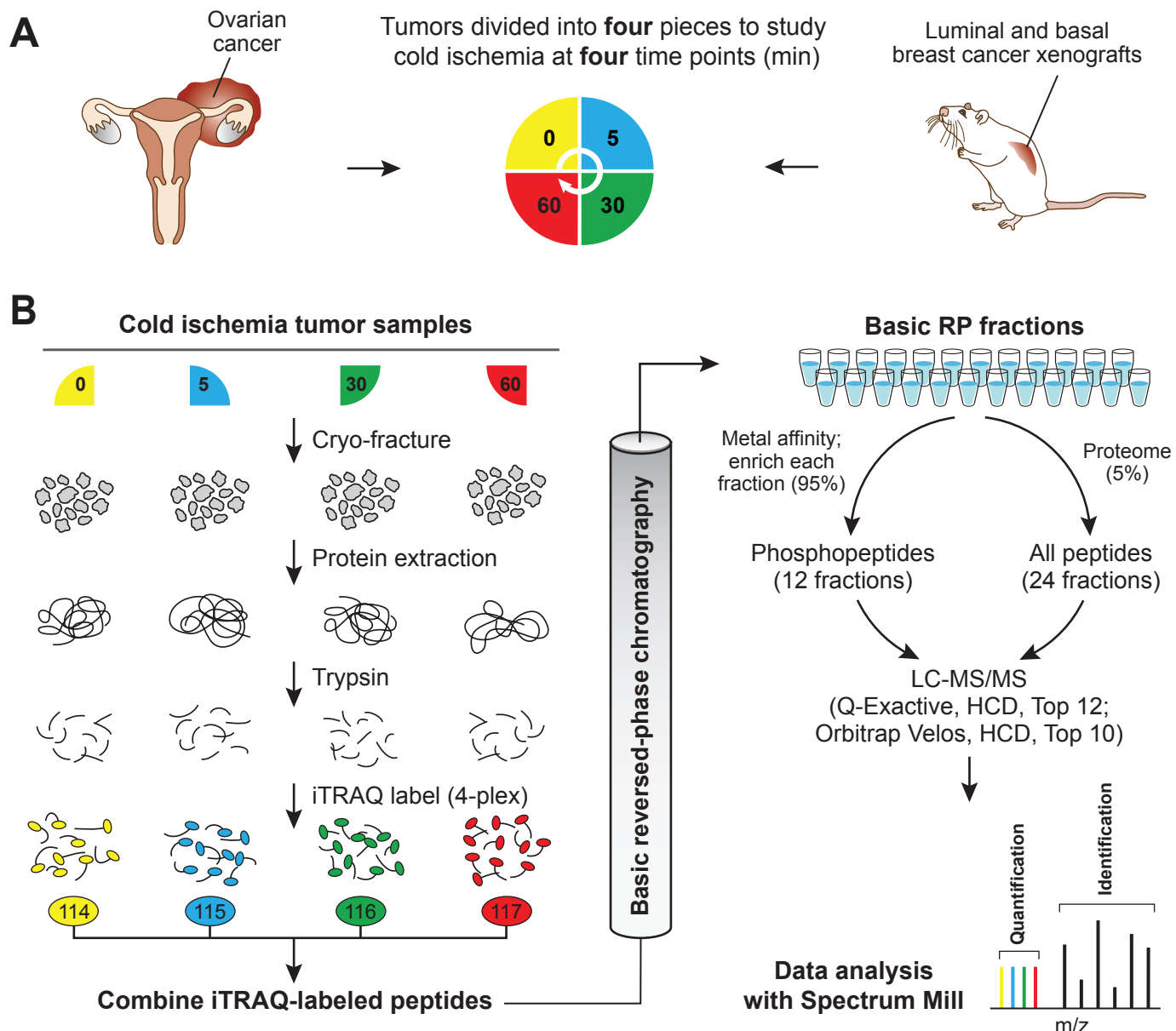


Figure 2:

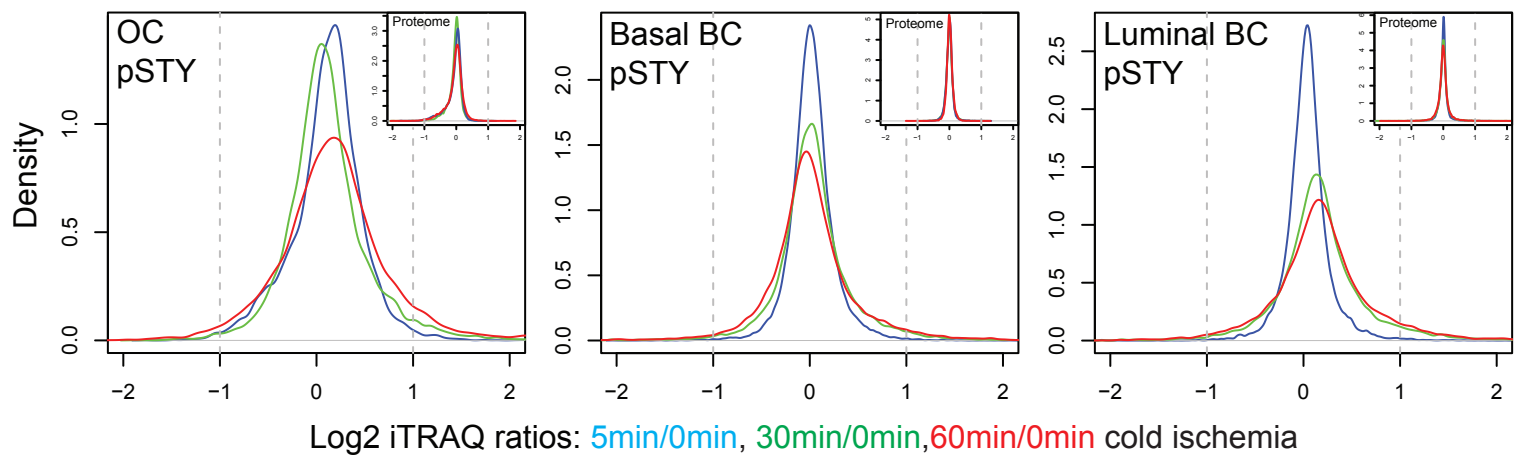


Figure 3:

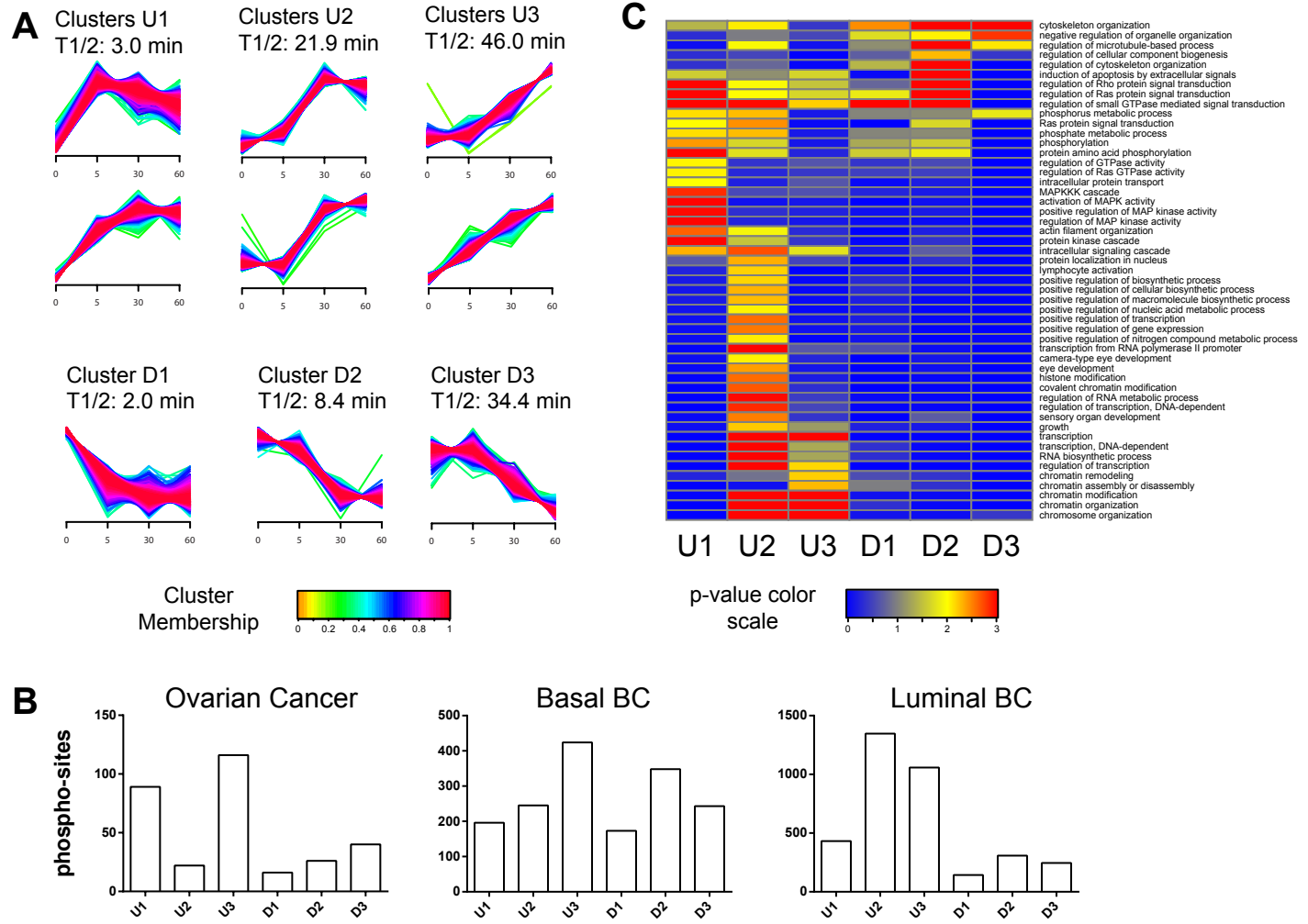


Figure 4:

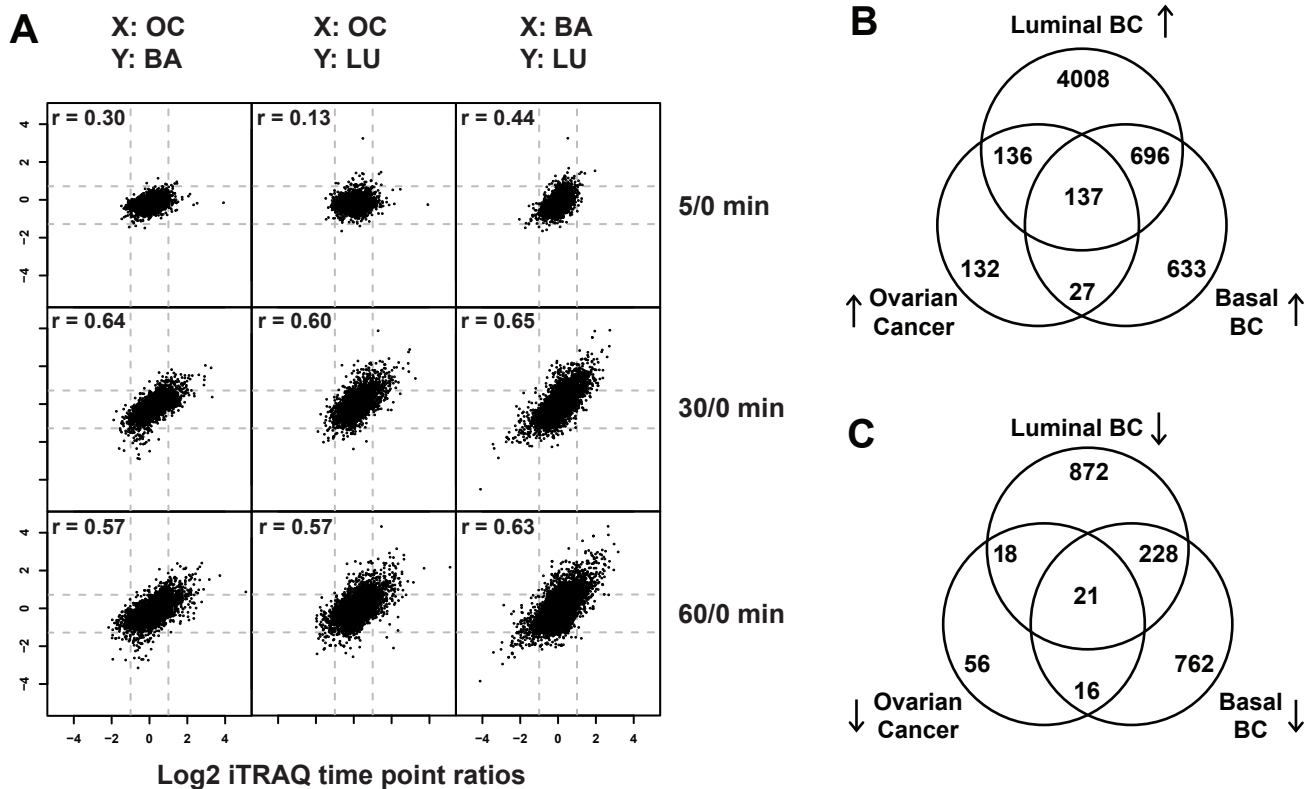
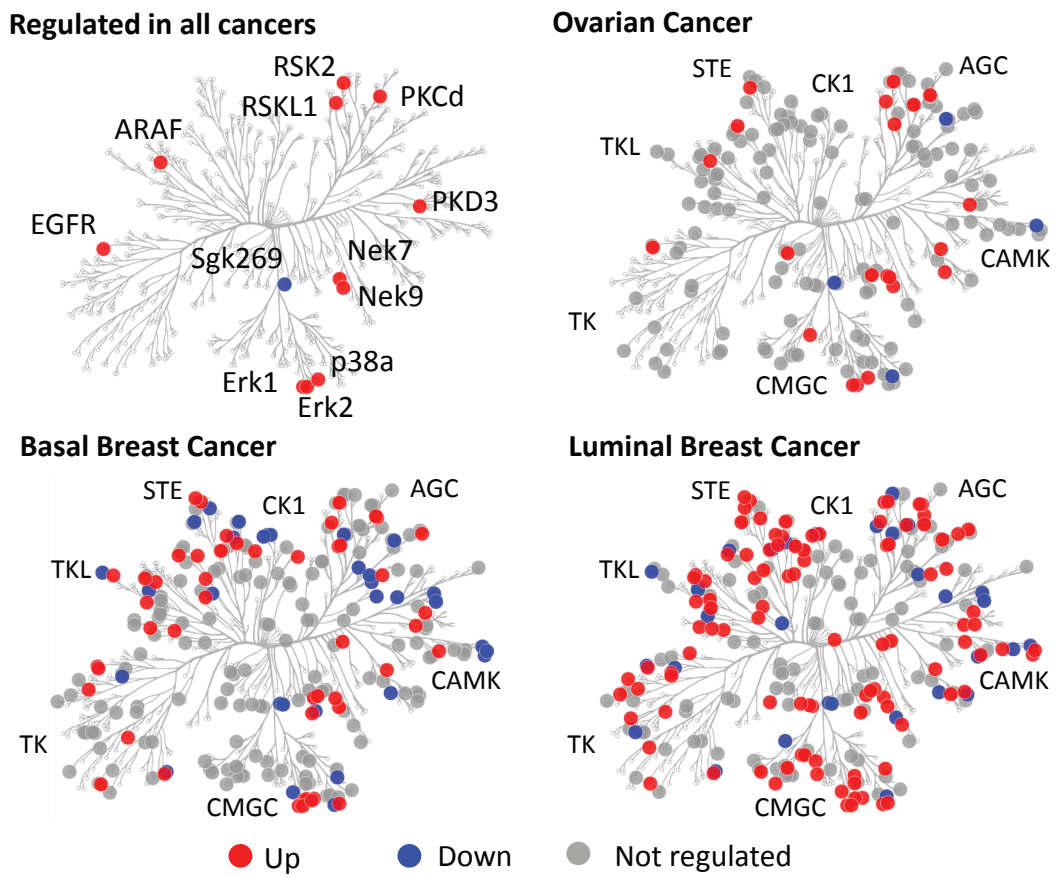


Figure 5:

A



B

